Science of the Total Environment 741 (2020) 140470

Contents lists available at ScienceDirect

Science of the Total Environment

journal homepage: www.elsevier.com/locate/scitotenv

Chemical composition and sources of submicron aerosol in a coastal city of China: Results from the 2017 BRICS summit study

Yanru Zhang [a,b,c], Lingling Xu [a,b,*], Mazhan Zhuang [d], Guoqing Zhao [a,b], Yuping Chen [a,b,c], Lei Tong [a,b], Chen Yang [a,b,c], Hang Xiao [a,b], Jinsheng Chen [a,b,*], Xin Wu [a,b,c], Youwei Hong [a,b], Mengren Li [a,b], Yahui Bian [a,b], Yanting Chen [a,b]

[a] Center for Excellence in Regional Atmospheric Environment, Institute of Urban Environment, Chinese Academy of Sciences, Xiamen 361021, China
[b] Key Laboratory of Urban Environment and Health, Institute of Urban Environment, Chinese Academy of Sciences, Xiamen 361021, China
[c] University of Chinese Academy of Sciences, Beijing 100086, China
[d] Xiamen Institute of Environmental Science, Xiamen, CN 361006, China

HIGHLIGHTS

- NM-PM_1 influenced by control and weather condition in a coastal city was studied.
- Emission control had significant effects on reducing traffic related pollutants.
- Long-range transport from continent enhanced sulfate contribution in control episodes.
- Calm weather conduced to the accumulation of nitrate and HOA even under control.

GRAPHICAL ABSTRACT

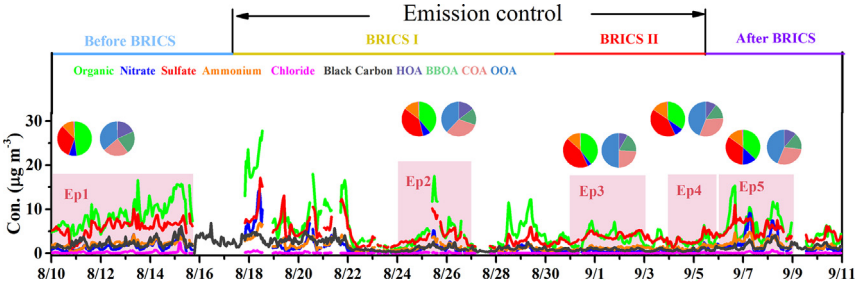

ARTICLE INFO

Article history:
Received 10 March 2020
Received in revised form 22 June 2020
Accepted 22 June 2020
Available online 24 June 2020

Editor: Jianmin Chen

Keywords:
Submicron particles
Aerosol chemistry
Source apportionment
ACSM
Xiamen BRICS

ABSTRACT

Chemical compositions of non-refractory submicron aerosol (NR-PM_1) were measured via an Aerodyne Aerosol Chemical Speciation Monitor at the coastal city Xiamen during the 2017 BRICS summit from August 10 to September 10. Mean hourly concentration of NR-PM_1 was 13.55 ± 8.83 μg m^{-3} during the study period, decreasing from 18.83 μg m^{-3} before-BRICS to 13.02 μg m^{-3} in BRCIS I and 8.42 μg m^{-3} in BRICS II. Positive matrix factor analyses resolved four organic aerosols (OA): a hydrocarbon-like OA (HOA, 14.78%), a cooking-related OA (COA, 28.21%), a biomass burning OA (BBOA, 18.00%), and an oxygenated OA (OOA, 39.22%). The contributions of local pollutants like nitrate and HOA reduced, while the proportions of sulfate and OOA increased during the control episodes. The diurnal patterns of NR-PM_1 species and OA components in each episode were characterized. The results showed that BC, nitrate, COA, and HOA had peaks in the morning and evening, which became less obvious under the emission control. Moreover, the diurnal variations of all species in Ep 3 with emission control were much flatter due to the effect of transport. Backward trajectories analysis confirmed the long-range transport of air masses from the continent, which resulted in the high proportions of sulfate (43.69%) and OOA (50.28%) in Ep 3. Our study implies the significant effect of emission control on reducing primary pollutants, but the formation of particles during the long-range transport need to be paid more attention when set the air quality control strategies in coastal cities.

* Corresponding authors at: Center for Excellence in Regional Atmospheric Environment, Institute of Urban Environment, Chinese Academy of Sciences, Xiamen 361021, China.
E-mail addresses: linglingxu@iue.ac.cn (L. Xu), jschen@iue.ac.cn (J. Chen).

https://doi.org/10.1016/j.scitotenv.2020.140470
0048-9697/

1. Introduction

Atmospheric aerosols have profound influences on human health, air quality, and the climate (Dockery et al., 1993; Poeschl, 2005). Submicron particles (PM_1, particles with a dynamic diameter less than 1 μm) in the atmosphere have become a crucial air pollutant in the urban environment for its strong extinction effect and high proportion in fine particles (Huang et al., 2010; Madronich and Flocke, 1999; Rivellini et al., 2017; Sun et al., 2016). Submicron particles are composed of complicated mixture of various species, and the organic components occupy a large fraction of submicron particles. Therefore, understanding of the chemical characteristics and sources of organic components in submicron particles are critical to enhance the efficiency of control strategies and model performances (Sun et al., 2018; Ulbrich et al., 2009).

China has experienced different kinds and degrees of air pollution events during the past decades. In recent years, many studies have qualified the role of emission control measures in air quality improvement in some megacities during the big events such as the 2014 Asia-Pacific Economic Cooperation (APEC) meeting and the 2008 Olympics game. Most studies focused on submicron particles were developed in the Beijing-Tianjin-Hebei region, the Yangtze River Delta region, and the Pearl River Delta region (Sun et al., 2018; Yong et al., 2017; Zhang et al., 2015; Zhou et al., 2018), but the studies focused on the coastal cities in southeast China were few. However, the pollution in coastal cities still exists (Yan et al., 2015). Xiamen, as one of the typical coastal cities in southeast China, has a sub-tropical climate. The influence of the special meteorological condition like typhoon and the high RH in Xiamen will result in different chemistry, sources, and formation mechanisms of NR-PM_1 from the inland cities in China. So far, the insight of the response of aerosol chemistry to emission control, transport and meteorology in coastal cities remains poorly understood. The international event of 2017 BRICS summit was hold in Xiamen during September 3–5. In order to improve the air quality during the summit, the government implemented a series of emission mitigation measures in Xiamen and its surrounding area since August 18, 2017. The mitigation measures covered the traffic, construction, industrial, and power plants emissions. Therefore, it is a precious opportunity to study the response of aerosol chemistry to control measures in the coastal environment and the result will help the government to design more effective aerosol control strategies in different regions.

In this study, the chemistry of submicron particles in the episodes, which happened in different emission control periods, was characterized by a high-resolution Aerosol Chemical Speciation Monitor (ACSM). The diurnal patterns and sources of organic aerosol were compared among different episodes to reflect the response of submicron particles chemistry to the emission controls of BRICS summit. The impacts of meteorological condition and transport of air masses on the characteristics of the PM_1 were also investigated in different episodes.

2. Experiments

2.1. Sampling site

The field observation was conducted in the Institute of Urban Environment, Chinese Academy of Sciences (IUECAS) in Xiamen (118°03′ E, 24°36′N, 80 m a.s.l). The observation site is located in Xiamen, with about 23 km northwest of the 2017 BRICS summit main event hall. This site is surrounded by two main roads and without obvious industrial sources. During the observation period, three zones were set up with different emission control intensities (Fig. S1). According to the distance from the main stadium of BRICS, the region surrounding Xiamen was set as the core emission control zone (Xiamen city), the strict emission control zone (Quanzhou and Zhangzhou cities), the general emission control zone (the remaining area of Fujian province). The neighboring provinces, like Zhejiang and Guangdong provinces were also under some emission controls.

2.2. Instruments

The major compositions of non-refractory submicron aerosol (NR-PM_1), including Organics (Org), Nitrate (NO_3), Sulfate (SO_4), Ammonium (NH_4), and Chloride (Chl), were measured using an Aerodyne ACSM from August 10 to September 10 in 2017. The detail of ACSM instrument operation can be found in previous studies (Ng et al., 2011; Sun et al., 2012; Tiitta et al., 2014). The time resolution of ACSM was about 15 min with a scan from m/z 10 to 150 amu (atomic mass unit) at 200 ms amu^{-1} rate.

Hourly PM_1 concentration was determined using a continuous particulate monitor (TEOM 1405-D, Thermo Co., USA) by the method of tapered element oscillating microbalance. Carbon oxide (CO), ozone (O_3), sulfur dioxide (SO_2), and nitrogen dioxide (NO_2) were obtained by gas analyzers (Thermo Fisher Scientific, Waltham, MA, USA). Black carbon (BC) was determined with model AE-31 Aethalometer (Magee Co., USA). The concentration of BC was detected at seven wavelengths (370, 470, 520, 590, 660, 880, and 950 nm) with a time resolution of 5 min, the BC concentration used in this study was at 880 nm. Meteorological parameters, including temperature (T), relative humidity (RH), pressures (P), wind direction (WD), wind speed (WS), and precipitation (Precip) were obtained from the Automatic air station of Xiamen.

2.3. ACSM data analysis and positive matrix factorization

The data of mass concentration of NR-PM_1 was analyzed with the standard Wave Metrics Igor Pro based data analysis software (version 6.37). The data analysis protocols referred to the previous studies (Sun et al., 2012). For instance, the collection efficiency (CE) for most species was 0.5. Then positive matrix factorization (PMF) was applied to explore the factors contributing to organic aerosol (OA) with the Igor Pro based PMF evaluation toolkit (PET) by analyzing the high-resolution mass spectra (Paatero and Tapper, 2010; Ulbrich et al., 2009). In this study, only values of $m/z < 120$ were used, while the values of $m/z > 120$ were discarded for two reasons: the fraction of the signals above $m/z > 120$ in the total signal was minor; the uncertainties of $m/z > 120$ were larger. The larger uncertainties of $m/z > 120$ were resulted by the low ion TE and the naphthalene signals have significant interferences on some high m/z's (Sun et al., 2012). The PMF solutions were evaluated by comparing the factors' mass spectral profiles, time series, and their correlation with some standard mass spectral profiles to obtain the optimal solution. Finally, a solution with four factors at $f_{peak} = 0$ was determined as optimal in this study. Four distinct factors included: a hydrocarbon-like OA (HOA), a cooking-related OA (COA), a biomass burning OA (BBOA), and an oxygenated OA (OOA).

2.4. Backward trajectory analysis

Hybrid Single-Particle Lagrangian Integrated Trajectory (HYSPLIT) developed by NOAA ARL was applied to evaluate the impacts of various source regions and transport pathway of air masses on Xiamen during different episodes (Draxler et al., 1997). 72 h backward trajectories were calculated every hour at a height of 100 m at IUECAS. The meteorological data with a resolution of 1° longitude × 1° latitude was obtained from the NCEP/GDAS. Cluster analysis was further applied for each episode using the total spatial variance (TSV) (Draxler et al., 2012).

3. Results and discussion

3.1. Overview of meteorology and submicron aerosol

Fig. 1 shows the time series of meteorology parameters (WD, WS, RH, T, and Precip), NR-PM_1 components (organics, nitrate, sulfate, ammonium, and chloride), and BC for the entire campaign from August 10 to September 10, 2017. The average T was 28.7 °C during the whole campaign varying from 22.9 to 34.8 °C, and the mean RH was

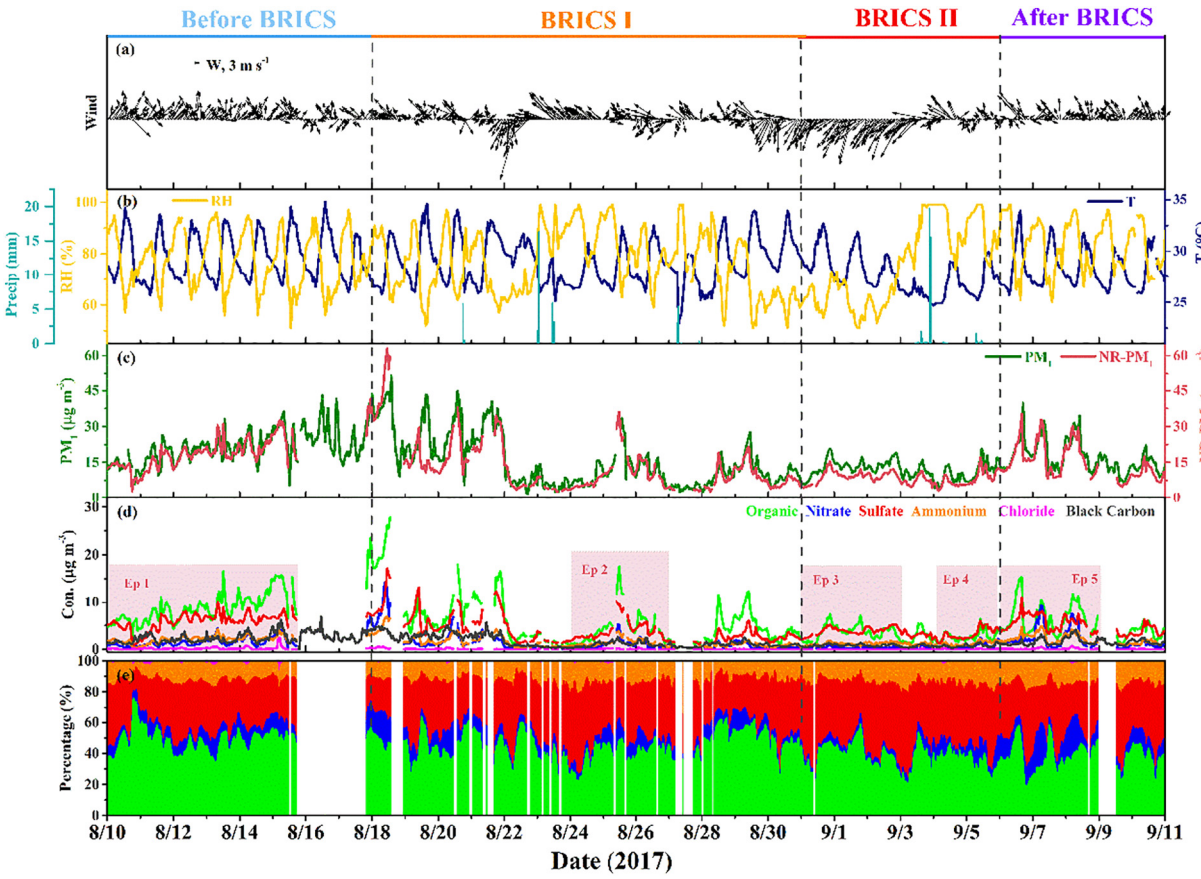

Fig. 1. Time series of (a) wind direction (WD) and wind speed (WS); (b) relative humidity (RH), temperature (T), and precipitation (Precip); (c) mass concentration of PM_1 and NR-PM_1, (d-e) mass concentration and fraction of chemical components in NR-PM_1.

77.6% with a range from 51.0 to 99.0%. Two obvious rainfalls happened during the whole observation period, one in the early morning of August 23 and the other in the evening of September 3. As shown in Fig. 1c, mass concentrations of NR-PM_1 measured by the ACSM agreed well with that of PM_1 measured by TEOM ($R^2 = 0.89$, slope = 0.98). Mean hourly concentration of NR-PM_1 was 13.55 ± 8.83 μg m^{-3}, varying from 1.88 to 63.12 μg m^{-3}. Such a significant variation might be contributed by emission control and meteorological conditions (Liang et al., 2017; Sun et al., 2013). Organics and sulfate were the two most abundant species in NR-PM_1 with average proportions of 42.17% and 36.42%, followed by ammonium (11.59%), nitrate (7.90%), and chloride (0.66%) (Fig. 1e). The superiority of organics and sulfate is in accord with the previous studies in Xiamen and other cities in China (Cao et al., 2017; Sun et al., 2016; Zhou et al., 2018). In order to examine the impacts of emissions control on the compositions of NR-PM_1, four periods were divided from the whole observation period according to emissions control program: before-BRICS (August 10–17), BRICS I (August 18–30), BRICS II (August 31–September 5), and after-BRICS (September 6–10). Before-BRICS represents the normal state without emission control. Mitigation measures to ensure the air quality were implemented in BRICS I and BRICS II. The mitigation was strengthened in BRICS II from the aspect of the reduction intensities of construction, traffic, industrial, and power plants emission. The amounts of emission reduction of SO_2, NO_X, CO, and PM in Xiamen increased from 19 to 41% in BRICS I to more than 40% in BRICS II (Table S1). Mean concentrations of NR-PM_1 during BRCIS I (13.02 μg m^{-3}) are of the same order of magnitude of those before-BRICS (18.83 μg m^{-3}) and after-BRICS (14.80 μg m^{-3}), but the value during BRICS II (8.42 μg m^{-3}) had significantly reduced. The lowest concentration of NR-PM_1 in BRICS II reflects the obvious effect of the emission control program. The significant effects of emission control on reducing the pollution of NR-PM_1 was also observed in other big events with emission control, like the 2015 China Victory Day parade, the APEC conference, and the 2016 G20 summit (Zhao et al., 2017; Li et al., 2018; Xu et al., 2015).

3.2. Chemical characteristics in different episodes

To further evaluate the evolution and sources of NR-PM_1 under different control conditions, five typical episodes were picked. Episode 1 (Ep 1, August 10–15) happened in before-BRICS and with sustainable growth of NR-PM_1, which represented the typical evolution of NR-PM_1 without control measures. Episode 2 (Ep 2, August 24–26) occurred in BRICS I, which represented the evolution of NR-PM_1 under the control measures. Episode 3 (Ep 3, August 31–September 2) was with lower concentration of NR-PM_1 and happened under strict emission control. Episode 4 (Ep 4, September 4–5) was not only under the influence of emission mitigation measures but also influenced by the severe tropical storm Mawar. Episode 5 (Ep 5, September 6–8) happened after BRICS was with few peaks of NR-PM_1, which could reflect the evolution of NR-PM_1 when the emission control ended.

3.2.1. Chemical compositions of NR-PM_1

As presented in Table 1, mean mass concentrations of NR-PM_1 showed comparable levels between Ep 1 and Ep 5 (18.34 μg m^{-3} versus 17.54 μg m^{-3}), which were higher than Ep 2 (10.98 μg m^{-3}), Ep 3 (9.18 μg m^{-3}), and Ep 4 (7.83 μg m^{-3}). In Ep 1, the dominant wind came from the southwest with a comparably low WS (mean value: 2.68 m s^{-1}, Fig. 1 and Table 1). Gaseous pollutants like SO_2, CO, and NO_2 (Fig. S2 and Table S1) were also higher in Ep 1. Hence, the evolution of NR-PM_1 in Ep 1 can be explained by the higher emission of pollutants

Table 1
Average values of meteorological parameters, mass concentrations of NR-PM_1 species, OA factors in the five episodes.

	Episode 1	Episode 2	Episode 3	Episode 4	Episode 5
Meteorological parameters					
T (°C)	29.5	28.4	28.7	26.9	28.6
RH (%)	77.4	83.4	62.4	89.7	83.3
WS (m s^{-1})	2.63	2.46	4.34	2.09	2.15
PM_1 species (μg m^{-3})					
NR-PM_1	18.34	10.98	9.18	7.83	17.54
Organics	8.69	4.55	3.72	2.71	6.59
Sulfate	5.85	3.92	3.91	3.19	5.70
Nitrate	1.49	0.98	0.34	0.70	2.62
Ammonium	2.11	1.45	1.18	1.18	2.48
Chloride	0.20	0.08	0.03	0.06	0.14
BC (μg m^{-3})	2.24	1.12	0.87	0.77	1.64
OA (μg m^{-3})					
HOA	1.56	0.59	0.31	0.27	0.74
BBOA	1.86	0.78	0.63	0.36	1.05
COA	2.07	1.39	0.89	0.87	1.89
OOA	3.14	1.74	1.90	1.17	2.84

and the unfavorable diffusion weather condition. Ep 2 was characterized by prevailing southeast winds with mean WS of 2.46 m s^{-1} and experienced calm weather condition like Ep 1. Gaseous pollutants (Table S2) in Ep 2 had different degrees of decrease comparing to Ep 1 due to the implement of emission mitigation measures. During August 24–25, the hourly concentration of NR-PM_1 showed a quick increase from 3.62 μg m^{-3} to 36.08 μg m^{-3} within only 35 h. Both Ep 3 and Ep 4 had lower mean concentrations of NR-PM_1, which reflects the high efficiency of strict emission control of BRICS II. It's worth mentioning that the weather condition was totally different between Ep 3 and Ep 4. The WD in Ep 3 was northeast and the higher WS (mean value: 4.34 m s^{-1}) presented a favorable diffusion condition. The prevailing wind in Ep 4 was the southwest wind and the mean WS was the lowest (2.09 m s^{-1}) among all episodes. As for Ep 5, the NR-PM_1 picked up quickly as a result of the stop of emission control and the calm weather condition (mean WS: 2.11 m s^{-1}).

Organics and sulfate comprised the major fraction of NR-PM_1 among all episodes with average percentages of 35–48% and 33–44%, respectively (Fig. 2). Average mass concentration (8.69 μg m^{-3}) and contribution (47.80%) of organics were highest in Ep 1. Comparing to Ep 1, the mean fraction of organics decreased in episodes under control (Ep 2, Ep 3, and Ep 4), and rebounded in Ep 5. This variation of organics contribution to NR-PM_1 was in consistent with the intensity of the emission reduction, which highlighted the effect of the mitigation measures on reduction of organics, such as the traffic and cooking released organics. As depicted in Fig. 2, contribution of sulfate in NR-PM_1 increased from Ep 1 (32.08%) to Ep 2 (39.04%), Ep 3 (43.68%), and Ep 4 (41.3%), then decreased to 34.73% in Ep 5. Sulfate is a well-known secondary pollutant, formed during the photo-oxidation of directly emitted sulfur dioxide (SO_2) species. High WS coming from the northeast direction in Ep 3 implied a long-range transport of air masses from the northeast continent. The formation of sulfate during the transport might be responsible for the high contribution of sulfate in Ep 3.

Average mass concentration of nitrate was higher in Ep 5 (2.62 μg m^{-3}) followed by Ep 1 (1.49 μg m^{-3}), Ep 2 (0.98 μg m^{-3}), Ep 4 (0.70 μg m^{-3}), and Ep 3 (0.34 μg m^{-3}). Rather low concentration of nitrate in Ep 3 was probably due to the strict emission control for traffic and the friendly diffusion condition. Differently from sulfate, the contribution of nitrate increased largely in Ep 4 (mean value: 7.06%) comparing to Ep 3 (3.59%). The different performance between sulfate and nitrate in Ep 3 and Ep 4 demonstrates the different evolution patterns of them. Unlike Ep 3, the WS in Ep 4 was the lowest and the RH was high (mean value: 89.37%). The unfavorable meteorological condition in Ep 4 would help the accumulation of local emission pollutants. From Fig. S2, the concentration of NO_2 significantly increased in the few days before Ep 4, which can explain some of the increase of nitrate in Ep 4. Specifically, the average concentration of nitrate in Ep 5 was more than twice of those in episodes with emission control. Simultaneously, the percentage nitrate (mean value: 12.97%) occupied in NR-PM_1 also reached its highest value in Ep 5. The highest loading of nitrate was in consistent with higher NO_2 in Ep 5 and reflects the significant importance of traffic emission on NR-PM_1 evolution after the summit.

Like sulfate and nitrate, mass concentration of ammonium showed a decreasing trend from Ep 1 to Ep 4, and then increased in Ep 5. Ammonium usually can combine with sulfate and nitrate in the atmosphere, so it is explicable that the higher proportion of ammonium increased from Ep 1 to Ep 3 like sulfate and the increase contribution in Ep 4 like nitrate. Chloride accounted for less than 2.50% in NR-PM_1. The concentration and contribution of Chloride were in the order of Ep 1 > Ep 5 > Ep 2 > Ep 4 > Ep 3. It is reported that the primary pollutant BC had high proportion in fine particles in Xiamen (Deng et al., 2020). The mean concentrations of BC were in ascending order of Ep 1, Ep 5, Ep 2, Ep 3, and Ep 4, which was well consistent with the extent of emission control.

3.2.2. Diurnal pattern of NR-PM_1 species

The diurnal variations of NR-PM_1 species and BC during different episodes are presented in Fig. 3. Numerous factors, such as photochemical production, gas-particle partitioning, local primary emissions, and

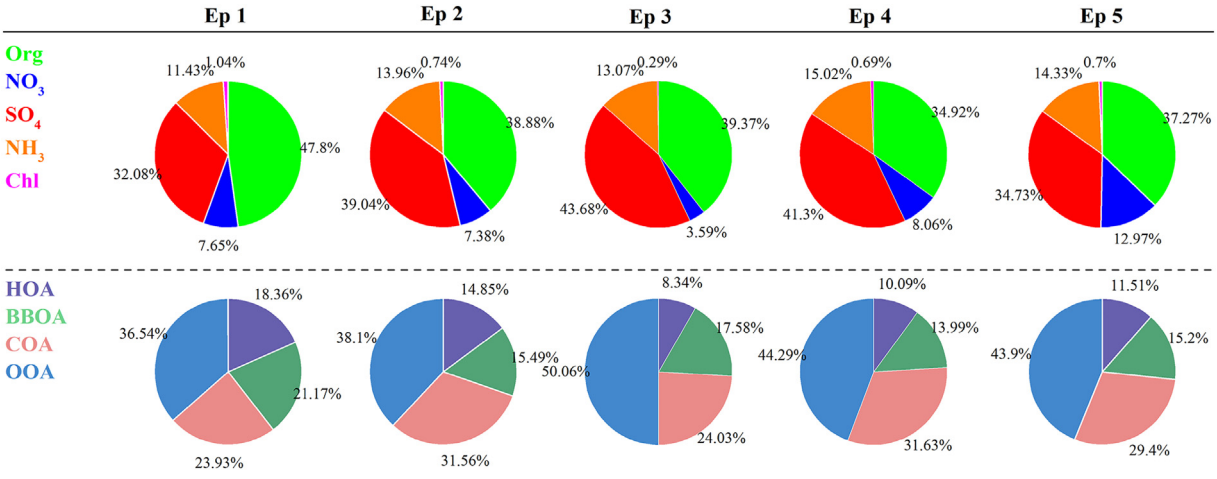

Fig. 2. Average mass fraction of NR-PM_1 species and OA species in the five episodes.

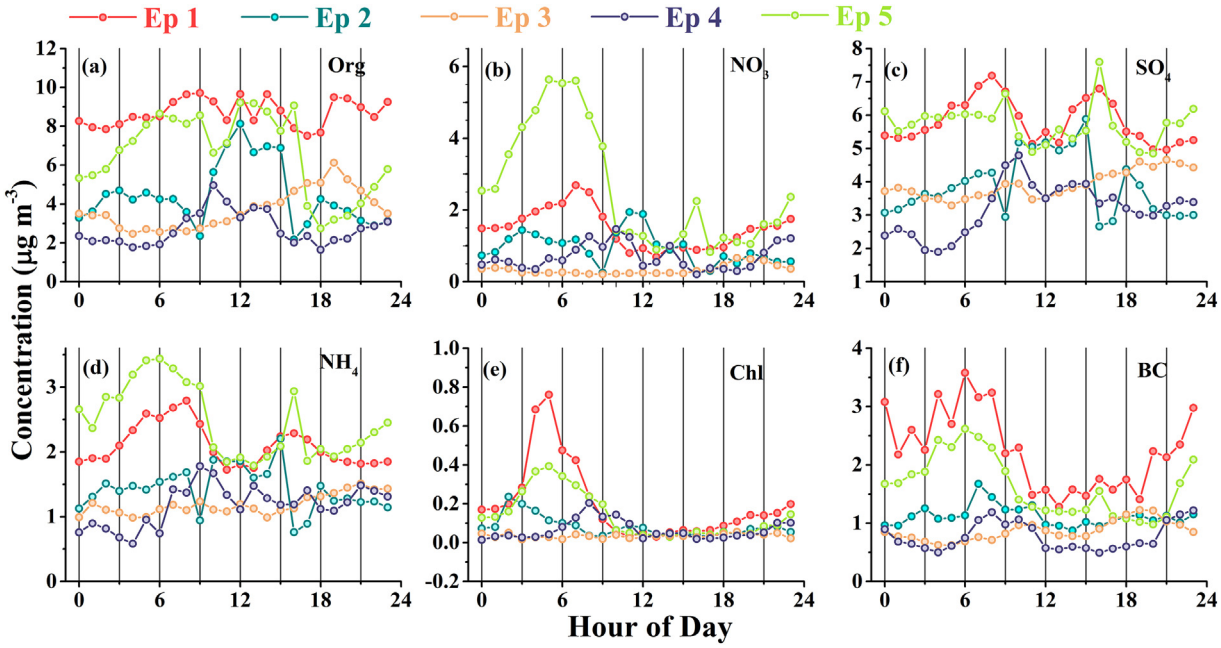

Fig. 3. Diurnal variations of NR-PM_1 species during the five episodes.

disperse condition can influence the diurnal pattern of NR-PM_1 species (Huang et al., 2012; Zhang et al., 2017). As a primary pollutant, BC showed double peaks in all episodes in the morning and evening. The diurnal pattern of BC in our study was similar with Hangzhou (Li et al., 2018), Shanghai (Huang et al., 2012), and Beijing (Huang et al., 2010). The lower concentration of BC in the afternoon to a certain extent can be attributed to the dilution effect of the higher planetary boundary layer (PBL) (Hu et al., 2017). The diurnal variation of BC was more obvious in Ep 1 and Ep 5, which reflects the influence of local emission on BC. In Ep 1, Ep 2, and Ep 5, three peaks in the diurnal pattern of organics were found in the breakfast time, lunch time, and dinner time, which proves the influence of cooking emission on the organics in Xiamen. Beyond the influence of cooking, the peaks of organics might also be contributed by traffic emission (HOA) and photochemical formation process (OOA) (Zhang et al., 2017). As for Ep 2 and Ep 4, the concentration of organics was obviously higher in the day time, which was likely due to the photochemical processing. The result could be supported by the quickly increase of O_3 in the daytime during Ep 2 and Ep 4 (Fig. S2). Whereas, the diurnal pattern of organics in Ep 3 was totally different from those in other periods. The long-range transport promoted by high WS and the strict emission control might influence the diurnal variation of organics in Ep 3.

The diurnal variations of nitrate were similar in Ep 1 and Ep 5 with two peaks in morning and evening, respectively, which reflects the influence of traffic in the episodes without emission control. The lower concentration of nitrate in the afternoon might be associated with the good vertical diffusion condition brought by the development of PBL. Flat diurnal variation of nitrate in Ep 3 highlights the obvious effect of emission mitigation of the summit. In addition, the beneficial diffusion condition and the long-range transport also could contribute to the flat diurnal variation of nitrate in Ep 3. The diurnal variation of nitrate in Ep 4 and Ep 2 also had visual peaks in the morning and evening, reflecting the influence of local emission on nitrate under calm weather condition even during the emission control period. Like nitrate, chloride also presented higher concentrations in the early morning and lower in the afternoon in most episodes except Ep 3, which can be contributed to the boundary layer variation and their volatility (Huang et al., 2012; Sun et al., 2016). In recent years, many studies had revealed that chloride in aerosol of coastal cities can react with N_2O_5 transform to $ClNO_2$ at nighttime, which can also explain some of the low concentration of chloride

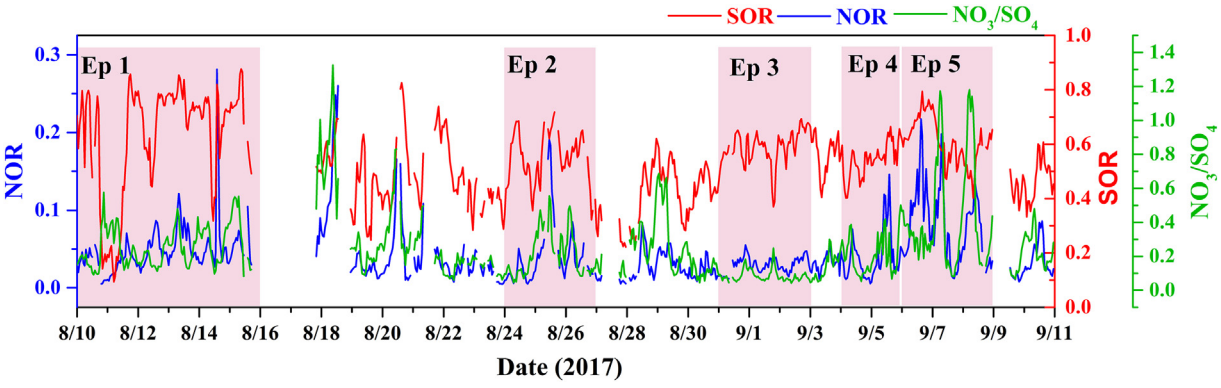

Fig. 4. Time series of SOR, NOR, and the ratio of NO_3/SO_4.

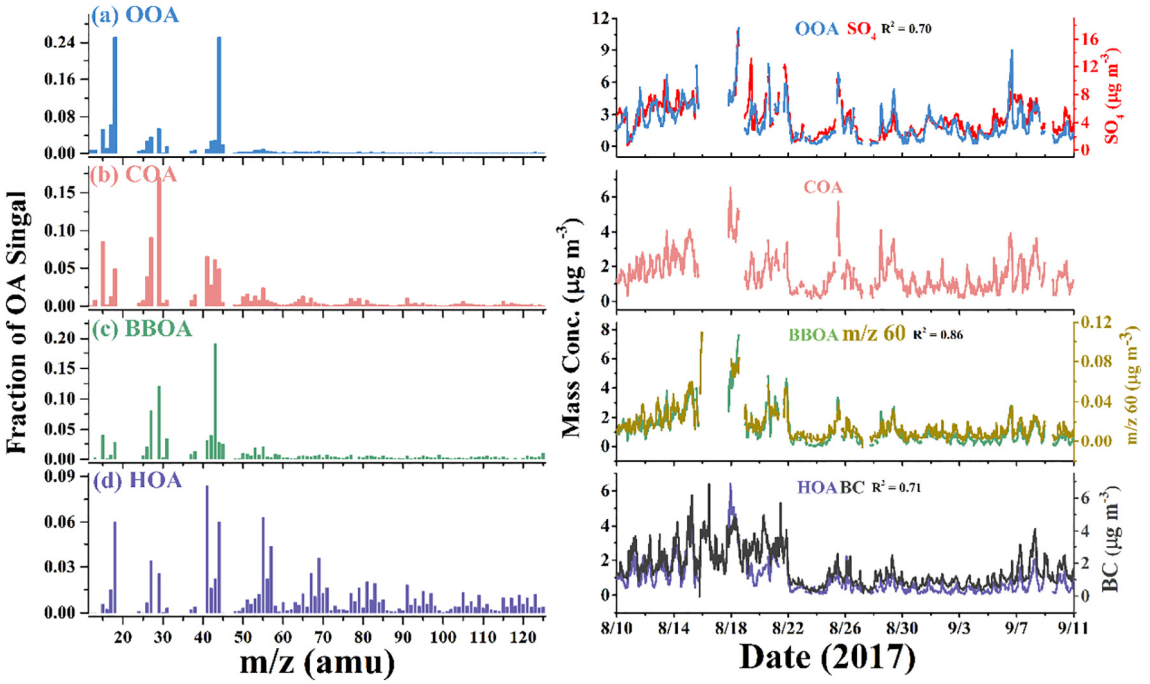

Fig. 5. Mass spectra of four OA factors (left panel), time series of OA factors and other tracers (right panel).

in nighttime (Osthoff et al., 2008; Saiz-Lopez and von Glasow, 2012; Wang et al., 2016).

Comparing to nitrate, the diurnal variation of sulfate was different. Two obvious peaks of sulfate were observed in the morning and afternoon for Ep 1 and Ep 5. As for the episodes under control, higher concentration of sulfate in the daytime than nighttime indicates its formation via photochemical pathways. However, the diurnal pattern of sulfate in Ep 3 was flat like other species. The diurnal profile of ammonium was the combined result of $(NH_4)_2SO_4$ and NH_4NO_3. It is worth to mention that, unlike other periods, Ep 2 and

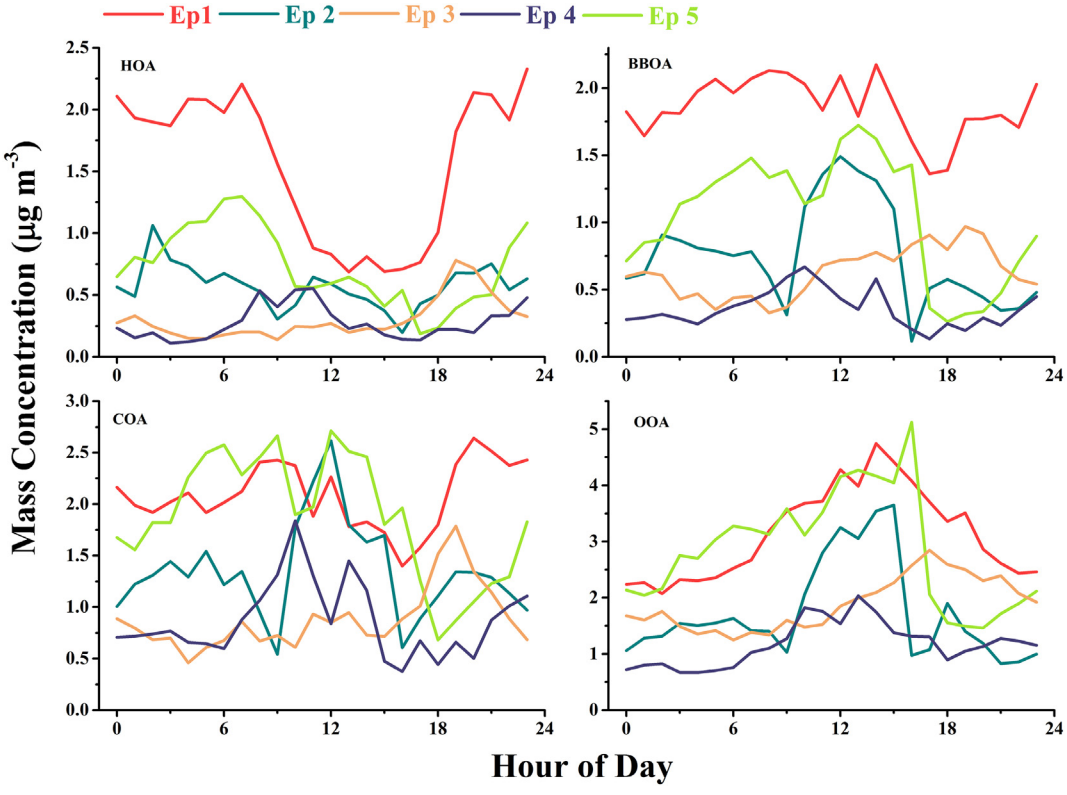

Fig. 6. Diurnal variations of OA components during the five episodes.

Ep 4 had high concentration of secondary inorganic aerosols (SIA, including sulfate, nitrate, and ammonium) at noon time. The result implies the enhanced secondary formation via photochemical process under the calm weather condition, which dominantly influenced the diurnal variation of sulfate in Ep 2 and Ep 4. In sum, the diurnal variations of all species were flatter in Ep 3, which could be associated with the reduction of emission and the effect of air masses transport.

3.3. Secondary inorganic aerosols formation

Secondary inorganic aerosols accounted for 21.69–81.23% of total NR-PM_1, with a mean proportion of 57.09%. The ratio of NO_3/SO_4 are usually used to evaluate the contributions of mobile and stationary sources. As presented in Fig. 4, the NO_3/SO_4 ratio was extremely low in Ep 3 (0.09) but higher in Ep 4 (0.21), indicating the increase contribution of local emission especially the mobile sources in Ep 4. The ratio of NO_3/SO_4 was the highest in Ep 5 (0.43). A substantially increase of NO_3/SO_4 ratio after the summit suggests the raised importance of mobile sources when emission control lifted.

Secondary reaction under the local atmosphere and the transport from other areas are usually treated as the major contributors to SIA. In order to learn more about the secondary formation of sulfate and nitrate, we calculated the sulfur oxidation ratio (SOR) and the nitrogen oxidation ratio (NOR). The calculation equations are as follows:

$$SOR = \frac{\left[SO_4^{2-}\right]}{\left[SO_4^{2-}\right] + [SO_2]}, \quad (1)$$

$$NOR = \frac{\left[NO_3^{-}\right]}{\left[NO_3^{-}\right] + [NO_2]}, \quad (2)$$

where [x] points to the molar concentration of x. Time series of SOR and NOR are given in Fig. 4. Mean value of NOR in the whole observation period was 0.04 ± 0.04, which was lower than the values observed in Nanjing (0.12 and 0.21) (Wu et al., 2018) and Hangzhou (0.05–0.15) (Ji et al., 2018). Mean NOR was highest in Ep 5 (0.08), while it was comparable in Ep 1 (0.05), Ep 2 (0.04), Ep 3 (0.03) and Ep 4 (0.04). The highest concentration of NO_2 (22.69 μg m^{-3}, Table S2) and the calm weather in Ep 5 can promote the oxidation of NO_2 and further resulted in high nitrate concentration (2.62 μg m^{-3}, Table 1). The comparable NOR among the Ep 1–4 implies that the concentration of NO_2 was the key factor influencing the formation of nitrate. Thus, for the episodes with calm weather (Ep 1, Ep 2, and Ep 4), the variation of nitrate concentration was well consistent with that of NO_2 concentration. SOR values varied with a mean value of 0.54 ± 0.15 in our observation period, and the difference among the five episodes was less (0.54–0.63). The SOR was higher in Xiamen than Beijing (< 0.3) (Sun et al., 2013), Hangzhou (<0.6) (Ji et al., 2018), which highlights a high atmospheric oxidative capacity during the observation period in Xiamen. Sulfate is more oxidized and aged species, and can be formed by oxidation of SO_2 in local or in the path of long-range transport. Differently from NOR, SOR was higher in Ep 3 (0.59) than Ep 4 (0.54) and the proportion of sulfate in Ep 3 was also a bit higher than Ep 4. The northeast wind with high WS in Ep 3 might indicate to the existence of the long-range transport of air masses from the continent, which will result in more input of sulfate. The influence of long-range transport on sulfate would be discussed in detail in section 3.5. Ep 4 happened closely after the Ep 3, the calm weather would slow down the diffusion efficiency of sulfate and resulted in the comparable contribution of sulfate in Ep 4. The reduced contribution of nitrate was also found during the emission control period of 2016 G20 summit and the 2015 China Victory Day parade. However, the increase contribution of sulfate was recorded in the control period of 2016 G20 summit, but the 2015 China Victory Day parade (Zhao et al., 2017; Li et al., 2018).

3.4. OA compositions and sources

In this study, four OA factors were identified by PMF analysis, including three primary OA factors (HOA, BBOA, COA), and one secondary OA factor (OOA). The mass spectra and time series of these four factors are shown in Fig. 5.

HOA usually comes from the primary traffic emissions linked with diesel and gasoline exhaust (Claudia et al., 2009). The mass spectrum of HOA is typically dominated by the $C_nH_{2n-1}^+$ ion series (m/z 27, 41, 55, 69, 83, 97) and $C_nH_{2n+1}^+$ ion series (m/z 29, 43, 57, 71, 99). The HOA mass spectrum is consistent with the previous studies conducted in urban areas (Claudia et al., 2009; Sun et al., 2016; Zhou et al., 2018). Higher concentrations of HOA were found in Ep 1 and Ep 5 than Ep 2–4 (Table 1). Contribution of HOA in Ep 1 (18.36%) was the highest, while the contributions ranged from 8.37% to 14.89% in other episodes (Fig. 1). The higher loading of HOA in Ep 1 conformed to the condition for no emission control on traffic in Ep 1. HOA correlated well with the tracer of combustion BC ($R^2 = 0.71$) throughout the whole observation period, reflecting the important source of traffic emission to HOA (Fig. 5). The correlation between HOA and BC was stronger in Ep 1 and Ep 5 ($R^2 = 0.69$ and 0.78) than in Ep 2–4 ($R^2 = 0.62$–0.63), which could be explained by the intense traffic emissions during Ep 1 and Ep 5. Previous studies had found that the regional transport could contribute to BC (Sun et al., 2014; Xu et al., 2014; Xu et al., 2015). Thus, the ratio of HOA/BC can reflect the relative importance of regional/long-range transport and local emission. The average HOA/BC was higher in Ep 1 (0.69), Ep 2 (0.52), and Ep 5 (0.43), while the ratios were only 0.34 and 0.35 in Ep 3 and Ep 4. The lowest ratio of HOA/BC in Ep 3 and Ep 4 was resulted from the increased contribution of regional/long-range transport of BC and the reduction of local emissions.

As depicted in Fig. 6, the diurnal pattern of HOA was resembled with BC and shared some similarity with nitrate either. In Ep 1 and Ep 5, the HOA diurnal cycles were similar, which had higher concentration since the late afternoon until the morning of the next day, and then decreased to its lowest concentration in the noontime. Besides PBL variation, the decrease of HOA in the day time might be attributed to the photochemical oxidation of HOA into oxidized secondary organic aerosol (SOA) (Li et al., 2018). The morning and evening peaks of the HOA diurnal pattern in Ep 1 and Ep 5 reflect the important influence of the traffic emission when no mitigation measure was implemented. It was obvious that the diurnal variation of HOA in episodes (Ep 2 to Ep 4) happened with the control of traffic emission was flatter. Although the traffic emission control in Ep 3 and Ep 4 were similar, the morning and evening peaks of HOA was more noticeable in Ep 4, which might be due to the suppressed diffusion of local emission pollutants in Ep 4.

The mass spectra of COA showed higher ratios of m/z 41/43 = 0.94 and m/z 55/57 = 4.09 than those of HOA (0.26 and 0.69), which were also reported in previous studies of ACSM and AMS (He et al., 2010; Lanz et al., 2010; Sun et al., 2016). COA had a high contribution of 28.21% to total OA during the whole observation period. The high contribution of COA was also characterized in other cities (Rivellini et al., 2017; Sun et al., 2011). Mean concentrations of COA were similar in Ep 1 and Ep 5, which were 23–57% higher than the values in the episodes happened under control (Ep 2–4). The government had shut down the restaurants without range hoods and forbade the open-air cooking activities like barbecues. On the other hand, all catering industries had been requested to use clean energy during the periods of BRICS I and BRICS II. Hence, this large reduction of COA in the episodes under the mitigation measures reflects the impact of the restriction on cooking. The diurnal cycle of COA showed three peaks in the breakfast, lunch, and dinner time, which was consistent with the cooking activities. However, there were still some differences among the episodes. Comparing to Ep 1, the peak of COA at lunch time was still obvious at noontime in Ep 2, Ep 3, and Ep 4, while the peaks in the breakfast and dinner or midnight snack time were small. This result was owed to the strict forbidden on the open-air cooking activities in the morning

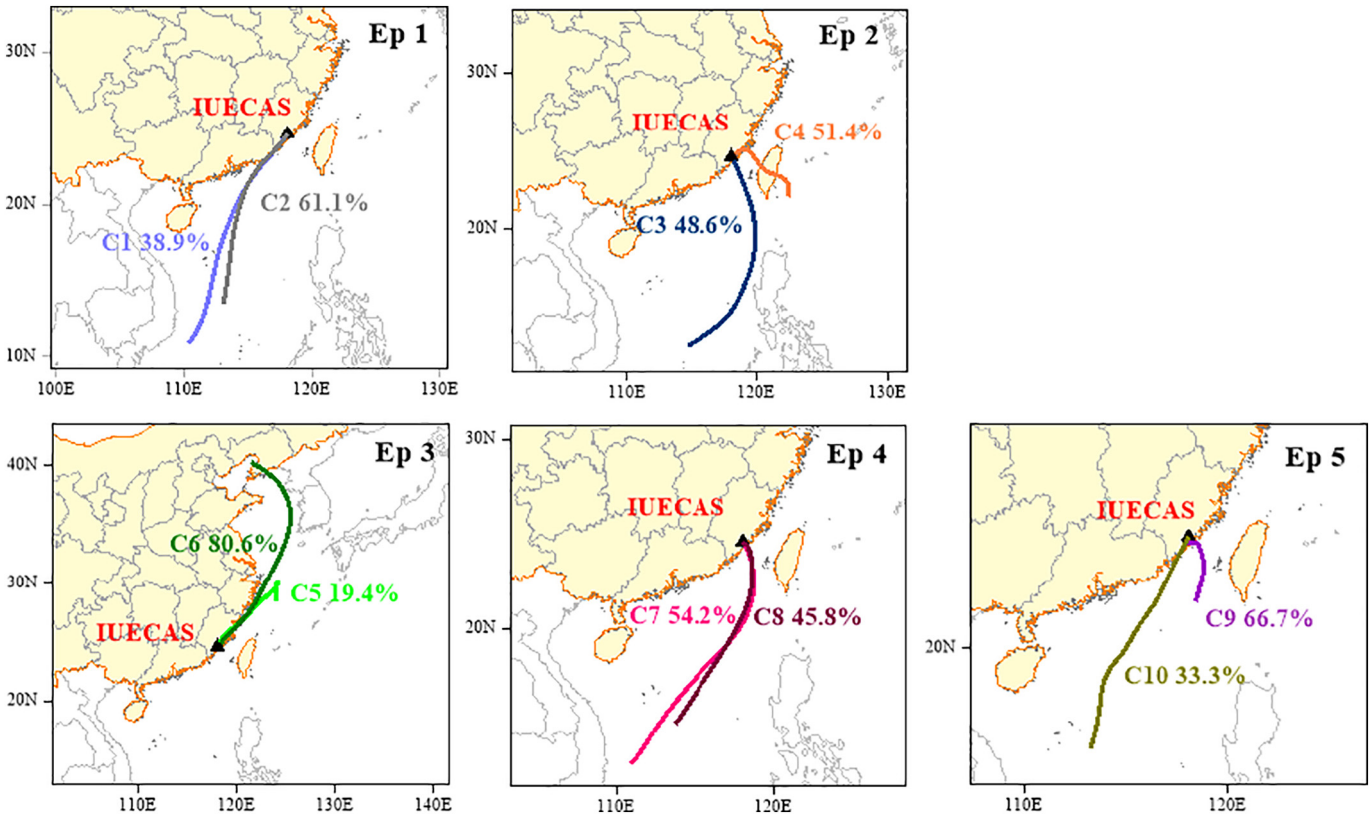

Fig. 7. 72 h-backward trajectories analyses for five episodes.

and evening. Both Ep 2 and Ep 4 were under unfavorable diffusion weather condition, but the more rigorous emission control in Ep 4 weakened the diurnal variation of COA.

BBOA spectrum showed relatively high loading in *m/z* 60 and 73 compared to other factors, and the correlation of BBOA with *m/z* 60 was strong ($R^2 = 0.86$) (Fig. 5). Previous studies also found pronounced peaks at m/z 60 and 73 in spectrum of BBOA (Cubison et al., 2011; Xu et al., 2015). As shown in Table 1, mass concentrations of BBOA were higher in Ep 1 (1.86 μg m^{-3}) and Ep 5 (1.05 μg m^{-3}), while the values decreased obviously in the episodes with emission controls (Ep 2: 0.78 μg m^{-3}, Ep 3: 0.63 μg m^{-3}, Ep 4: 0.36 μg m^{-3}). This result could be associated with the effect of the control about the biomass burning like straw burning. Contribution of BBOA to OA was the highest in Ep 1 (21.17%), followed by Ep 3 (17.46%), Ep 2 (15.53%), Ep 5 (15.20%), and Ep 4 (14.11%). Specifically, BBOA had higher concentration and contribution to OA in Ep 3 than Ep 4. The result suggests that the wind coming from the northeast direction with higher WS in Ep 3 could transport more BBOA to Xiamen.

According to the degree of ageing, SOA can be divided into less oxidized SOA (LO-OOA) and more oxidized SOA (MO-OOA). However, in this study, we failed to separate them and only one oxygenated OA (OOA) was found. The mass spectrum of OOA in this study was characterized by the prominent peaks at m/z 44 (25.13% of total OOA signal), which was consistent with the previous studies in other cities (Crippa et al., 2013; Zhang et al., 2015). What's more, the high ratio of m/z 44 in the mass spectrum indicates that SOA was highly oxidized in Xiamen. Mean concentrations of OOA were higher in Ep 1 (3.14 μg m^{-3}) and Ep 5 (2.84 μg m^{-3}) than the episodes (Ep 2: 1.74 μg m^{-3}, Ep 3: 1.90 μg m^{-3}, Ep 4: 1.17 μg m^{-3}) happened with emission control. The reduction of OOA from Ep 1 to Ep 2 and Ep 4 manifests the effect of emission mitigation measures from the regional scale. However, the contribution of OOA was the highest in Ep 3 (50.28%). As mentioned above, the transport of air masses came from the northeast continent in Ep 3 and OOA could come from the transport pathway. The diurnal pattern of OOA presented a higher level during the period of 12:00–16:00 among all episodes except Ep 3 (Fig. 6), indicating the contribution of photochemical processes to the formation of OOA. The different diurnal pattern of OOA in Ep 3 might be attributed to the impact of regional transport. As shown in Fig. 5, time series of OOA and sulfate presented high similarity. The correlation between OOA and sulfate were stronger in Ep 2 and Ep 4 ($R^2 = 0.88$ and 0.61), following by Ep 1, Ep 5 and Ep 3 ($R^2 = 0.45$, 0.38, and 0.35). Previous studies analyzed the correlation between OOA and O_X ($O_3 + NO_2$) to see the influence of photochemical process on the formation of OOA (Li et al., 2018). Table S4 presents the relative coefficient of O_X, OOA, and sulfate in each episode. The correlation of O_X with OOA were stronger than sulfate in all episodes, which suggests that OOA was more influenced by the photochemical process than sulfate. The speculation was supported by the diurnal pattern of OOA and sulfate under the normal state. OOA had a peak at noon, while sulfate had obvious peaks in the morning and afternoon (Fig. 6). The lowest correlation between OOA and sulfate in Ep 3 was likely associated with the transport of air masses. The episodes other than Ep 3 were all characterized by calm weather condition. The correlation between OOA and sulfate was closer in Ep 2 and Ep 4 than in Ep 1 and Ep 5, which might be attributed to the reduction of emission sources of precursors.

3.5. Effects of regional transport on different episodes

Fig. 7 presents the cluster analysis of backward trajectories in Xiamen, and two clusters were obtained for each episode. Ep 1 was dominated by the air masses (C1: 38.89% and C2: 61.11%) coming from the southwest of Xiamen. The air masses passed above the sea surface, through the Guangdong province and the southeast of Fujian province. Previous studies had revealed that local emissions and long-range transport were the two major reasons for the accumulation of air pollutants in coastal regions (Cao et al., 2017; Tsai et al., 2010). C1 and C2 in Ep 1 had long transport pathway on the sea surface, which might not bring

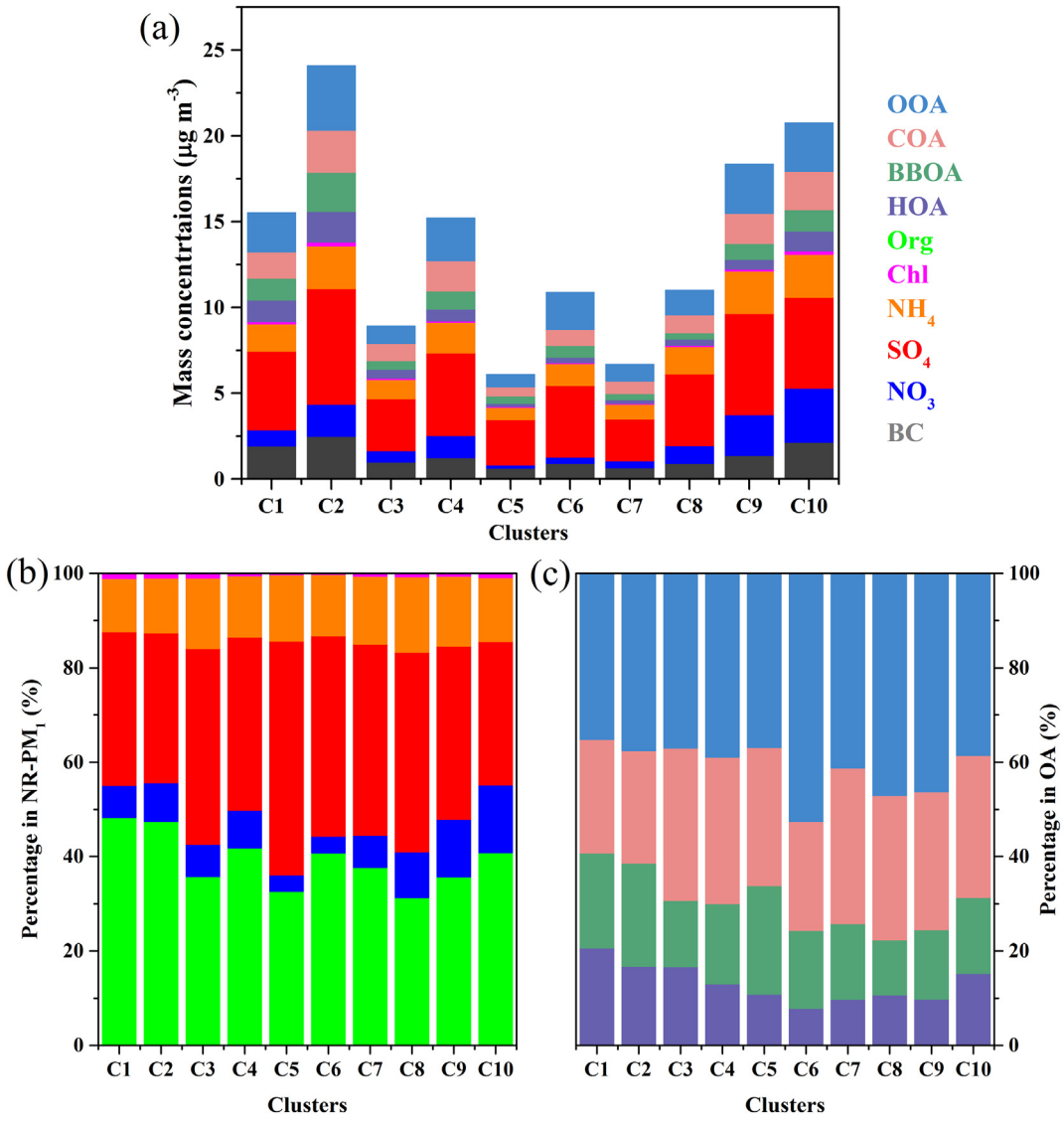

Fig. 8. Mass concentrations (a) of NR-PM_1 and OA components in different clusters; percentages of NR-PM_1 species (b) and OA species (c) in different clusters.

much pollutants to Xiamen. Therefore, the high loading of nitrate, HOA, and BBOA associating with C1 and C2 in Ep 1 were probably caused by local emissions (Fig. 8).

The air masses coming to Xiamen in Ep 2 could be divided into two groups, one (C3: 48.61%) was with a long transport pathway from the sea surface of the southwest direction, another (C4: 51.39%) was coming from the Taiwan Province and with a short transport pathway. Half of the airmasses transported in a short distance confirms the calm weather in Ep 2 as mentioned above. Mass concentrations of NR-PM_1 and nitrate in C4 were almost twice of C3 (Fig. 8), which suggests the impact of local emission and accumulation on NR-PM_1 in Ep 2.

Ep 3 was dominated by the long-range transport of air masses from the Northeast China (C6, 80.56%), which confirmed above speculation about air masses transport in Ep 3. The remaining of air masses in Ep 3 were originated from the Yangtze River Delta region. Clusters coming from the northeast with longer transport pathway tended to contribute more sulfate and OOA. Specifically, there were the highest contribution of sulfate (49.49%) in C5 and OOA (52.88%) in C6 among all clusters. Additionally, the contribution of BBOA in OA was higher in C5 than in other clusters. The air masses of Ep 4 (C7: 54.25% and C8: 45.75%) were all coming from the sea surface of the southwest of Xiamen. Although the restriction of emission in Ep 4 was in common with Ep 3, nitrate contribution was larger in C7 and C8 (6.80% and 9.67%) than in C5 and C6 (3.53% and 3.60%). The transport directions of air masses can explain most of the different contributions of the NR-PM_1 species in Ep 3 and Ep 4.

One short cluster (C9: 66.79%) originated from the Taiwan strait and one longer cluster (C10: 33.3%) came from the sea surface of southwest with a transport path above the south of Fujian province were found in Ep 5. High occurrence of short-range transport confirmed the calm weather in Ep 5. It was obvious that the mass concentration of NR-PM_1 were higher in C9 and C10. Additionally, C10 had highest contribution of HOA (15.24% in OA) and nitrate (14.26% in NR-PM_1). Since the transport of airmasses over the sea surface of the South China Sea did not bring much pollutants, the local emissions were probably responsible for the growth of NR-PM_1 when emission control ended.

On the whole, the air masses in Ep 1, Ep 2, Ep 4, and Ep 5 generally transported over sea surface from the southwest direction, the NR-PM_1 of the above episodes were characterized by increase contribution of HOA and nitrate, which was largely due to the local emission and calm weather condition. In contrast, the air masses in Ep 3 transported from the northeast continents, which resulted in the high contributions of OOA and sulfate to NR-PM_1. The study of Li et al. (2018) had found that the regional transport increased the contribution of SIA even strict

emission control was implemented in Hangzhou, which is consistent with our result. Therefore, it is necessary to put attention on the transport of pollutants, which will help to ensure a better effect of implementation of emission mitigation.

4. Conclusions

In situ observation of NR-PM_1 was conducted by a high-resolution ACSM from August 10 to September 10, which was covered the 2017 BRICS summit in Xiamen. Mean hourly concentration of NR-PM_1 reduced from 18.83 μg m^{-3} before-BRICS to 13.02 μg m^{-3} in BRICS I and 8.42 μg m^{-3} in BRICS II. Contributions of local pollutants like nitrate and HOA reduced from 7.56% and 18.36% in Ep 1 to 3.59–7.38% and 8.37–14.89% in Ep 2–4, respectively. Additionally, the peaks of BC, nitrate, COA, and HOA in the morning and evening became less obvious under the emission control. The results indicated the significant effects of control measures, like for traffic and for open-air cooking, on the reduction of primary pollutants.

The higher SOR and lower NOR was observed in Xiamen as compared to other cities in China. The comparable NOR among the Ep 1–4 implied that the concentration of NO_2 was the key factor influencing the formation of nitrate. The difference of SOR among the episodes was also small. The increased contribution of sulfate in Ep 3 (43.68%) was associated with the transport of air masses promoted by high WS. OOA presented a higher level at noon under the calm weather, indicating the contribution of photochemical process to the formation of OOA. Although the concentration of NR-PM_1 largely decreased in Ep 3 under the strict emission control, the transport of airmasses from the northeast continents would result in the high proportions of OOA, BBOA, and sulfate in NR-PM_1. Thus, the emissions and the formation of particles during the transport need to be paid more attention when set the air quality control strategies in coastal cities.

CRediT authorship contribution statement

Yanru Zhang: Conceptualization, Methodology, Software, Investigation, Writing - review & editing.**Lingling Xu:**Conceptualization, Writing - review & editing.**Mazhan Zhuang:**Conceptualization, Supervision. **Guoqing Zhao:**Data curation.**Yuping Chen:**Writing - original draft.**Lei Tong:**Data curation.**Chen Yang:**Writing - original draft.**Hang Xiao:** Data curation.**Jinsheng Chen:**Conceptualization, Supervision, Writing - review & editing.**Xin Wu:**Investigation.**Youwei Hong:**Writing - original draft.**Mengren Li:**Writing - original draft.**Yahui Bian:**Investigation. **Yanting Chen:**Investigation.

Declaration of competing interest

The authors declare that they have no known competing financial interests or personal relationships that could have appeared to influence the work reported in this paper.

Acknowledgements

This study was funded by the National Key Research and Development Program (2016YFC02005 & 2016YFE0112200), the National Natural Science Foundation of China (41575146), the Chinese Academy of Sciences Interdisciplinary Innovation Team Project, and the Natural Science Foundation of Fujian Province, China (2016J01201).

Appendix A. Supplementary data

Supplementary data to this article can be found online at https://doi.org/10.1016/j.scitotenv.2020.140470.

References

Cao, L., Zhu, Q., Huang, X., Deng, J., Chen, J., Hong, Y., Xu, L., He, L., 2017. Chemical characterization and source apportionment of atmospheric submicron particles on the western coast of Taiwan Strait, China. J. Environ. Sci. 52, 293–304.

Claudia, M., Alex, H., Cubison, M.J., Aiken, A.C., Docherty, K.S., Kimmel, J.R., Ulbrich, I.M., Michael, H., Jimenez, J.L., 2009. Characterization of primary organic aerosol emissions from meat cooking, trash burning, and motor vehicles with high-resolution aerosol mass spectrometry and comparison with ambient and chamber observations. Environmental Science & Technology 43, 2443–2449.

Crippa, M., DeCarlo, P., Slowik, J., Mohr, C., Heringa, M., Chirico, R., Poulain, L., Freutel, F., Sciare, J., Cozic, J., 2013. Wintertime aerosol chemical composition and source apportionment of the organic fraction in the metropolitan area of Paris. Atmos. Chem. Phys. 13, 961–981.

Cubison, M., Ortega, A., Hayes, P., Farmer, D., Day, D., Lechner, M., Brune, W., Apel, E., Diskin, G., Fisher, J., 2011. Effects of aging on organic aerosol from open biomass burning smoke in aircraft and laboratory studies. Atmos. Chem. Phys. 11, 12049–12064.

Deng, J., Zhao, W., Wu, L., Hu, W., Ren, L., Wang, X., Fu, P., 2020. Black carbon in Xiamen, China: temporal variations, transport pathways and impacts of synoptic circulation. Chemosphere 241, 125133.

Dockery, D.W., Pope, C.A., Xu, X., Spengler, J.D., Ware, J.H., Fay, M.E., Ferris, B.G., Speizer, F.E., 1993. An association between air pollution and mortality in six U.S. cities. N. Engl. J. Med. 329, 1753.

Draxler, R.R., Hess, G.D., Draxler, R.R., 1997. Description of the Hysplit_4 Modeling System, National Oceanic & Atmospheric Administration Technical Memorandum Erl Arl. pp. 197–199.

Draxler, R., Stunder, B., Rolph, G., Stein, A., Taylor, A., 2012. HYSPLIT4 user's Guide, Version 4, Report. NOAA, Silver Spring, Md.

He, L.-Y., Lin, Y., Huang, X.-F., Guo, S., Xue, L., Su, Q., Hu, M., Luan, S.-J., Zhang, Y.-H., 2010. Characterization of high-resolution aerosol mass spectra of primary organic aerosol emissions from Chinese cooking and biomass burning. Atmos. Chem. Phys. 10, 11535–11543.

Hu, W., Hu, M., Hu, W.W., Zheng, J., Chen, C., Wu, Y., Guo, S., 2017. Seasonal variations in high time-resolved chemical compositions, sources, and evolution of atmospheric submicron aerosols in the megacity Beijing. Atmos. Chem. Phys. 17, 9979–10000. https://doi.org/10.5194/acp-17-9979-2017.

Huang, X.F., He, L.Y., Hu, M., Canagaratna, M.R., Sun, Y., Zhang, Q., Zhu, T., Xue, L., Zeng, L.W., Liu, X.G., Zhang, Y.H., Jayne, J.T., Ng, N.L., Worsnop, D.R., 2010. Highly time-resolved chemical characterization of atmospheric submicron particles during 2008 Beijing Olympic games using an aerodyne high-resolution aerosol mass spectrometer. Atmos. Chem. Phys. 10, 8933–8945.

Huang, X.F., He, L.Y., Xue, L., Sun, T.L., Zeng, L.W., Gong, Z.H., Hu, M., Zhu, T., 2012. Highly time-resolved chemical characterization of atmospheric fine particles during 2010 Shanghai World Expo. Atmos. Chem. Phys. 12, 4897–4907.

Ji, Y., Qin, X., Wang, B., Xu, J., Shen, J., Chen, J., Huang, K., Deng, C., Yan, R., Xu, K., 2018. Counteractive effects of regional transport and emission control on the formation of fine particles: a case study during the Hangzhou G20 summit. Atmos. Chem. Phys. 18, 13581–13600.

Lanz, V.A., Prévôt, A.S.H., Alfarra, M.R., Weimer, S., Mohr, C., DeCarlo, P.F., Gianini, M.F.D., Hueglin, C., Schneider, J., Favez, O., D'Anna, B., George, C., Baltensperger, U., 2010. Characterization of aerosol chemical composition with aerosol mass spectrometry in Central Europe: an overview. Atmos. Chem. Phys. 10, 10453–10471.

Li, K., Chen, L., White, S.J., Zheng, X., Lv, B., Lin, C., Bao, Z., Wu, X., Gao, X., Ying, F., 2018. Chemical characteristics and sources of PM 1 during the 2016 summer in Hangzhou☆. Environ. Pollut. 232, 42–54.

Liang, P., Tong, Z., Fang, Y., Li, Y., Wang, J., 2017. The role of meteorological conditions and pollution control strategies in reducing air pollution in Beijing during APEC 2014 and parade 2015. Atmospheric Chemistry & Physics 17, 1–62.

Madronich, S., Flocke, S., 1999. The Role of Solar Radiation in Atmospheric Chemistry, Environmental Photochemistry. Springer, pp. 1–26.

Ng, N.L., Herndon, S.C., Trimborn, A., Canagaratna, M.R., Croteau, P.L., Onasch, T.B., Sueper, D., Worsnop, D.R., Zhang, Q., Sun, Y.L., 2011. An aerosol chemical speciation monitor (ACSM) for routine monitoring of the composition and mass concentrations of ambient aerosol. Aerosol Sci. Technol. 45, 780–794.

Osthoff, H.D., Roberts, J.M., Ravishankara, A.R., Williams, E.J., Lerner, B.M., Sommariva, R., Bates, T.S., Coffman, D., Quinn, P.K., Dibb, J.E., 2008. High levels of nitryl chloride in the polluted subtropical marine boundary layer. Nat. Geosci. 1, 324–328.

Paatero, P., Tapper, U., 2010. Positive matrix factorization: a non-negative factor model with optimal utilization of error estimates of data values. Environmetrics 5, 111–126.

Poeschl, U., 2005. Atmospheric aerosols: composition, transformation, climate and health effects. Angew. Chem. Int. Ed. 44, 7520–7540.

Rivellini, L.-H., Chiapello, I., Tison, E., Fourmentin, M., Féron, A., Diallo, A., N'Diaye, T., Goloub, P., Canonaco, F., Prévôt, A.S.H., 2017. Chemical characterization and source apportionment of submicron aerosols measured in Senegal during the 2015 SHADOW campaign. Atmospheric Chemistry & Physics 17.

Saiz-Lopez, A., von Glasow, R., 2012. Reactive halogen chemistry in the troposphere. Chem. Soc. Rev. 41, 6448.

Sun, Y.-L., Zhang, Q., Schwab, J., Demerjian, K., Chen, W.-N., Bae, M.-S., Hung, H.-M., Hogrefe, O., Frank, B., Rattigan, O., 2011. Characterization of the sources and processes of organic and inorganic aerosols in New York city with a high-resolution time-of-flight aerosol mass apectrometer. Atmos. Chem. Phys. 11, 1581–1602.

Sun, Y., Wang, Z., Dong, H., Yang, T., Jie, L., Pan, X., Ping, C., Jayne, J.T., 2012. Characterization of summer organic and inorganic aerosols in Beijing, China with an aerosol chemical speciation monitor. Atmos. Environ. 51, 250–259.

Sun, Y., Wang, Z., Fu, P., Jiang, Q., Yang, T., Li, J., Ge, X., 2013. The impact of relative humidity on aerosol composition and evolution processes during wintertime in Beijing, China. Atmos. Environ. 77, 927–934.

Sun, Y., Jiang, Q., Wang, Z., Fu, P., Li, J., Yang, T., Yin, Y., 2014. Investigation of the sources and evolution processes of severe haze pollution in Beijing in January 2013. Journal of Geophysical Research: Atmospheres 119, 4380–4398.

Sun, C., Lee, B.P., Huang, D., Li, Y.J., Schurman, M.I., Louie, P.K.K., Luk, C., Chan, C.K., 2016. Continuous measurements at the urban roadside in an Asian megacity by aerosol chemical speciation monitor (ACSM): particulate matter characteristics during fall and winter seasons in Hong Kong. Atmospheric Chemistry & Physics 15, 19405–19445.

Sun, Y., Xu, W., Zhang, Q., Jiang, Q., Canonaco, F., Prévôt, A.S., Fu, P., Li, J., Jayne, J., Worsnop, D.R., 2018. Source apportionment of organic aerosol from 2-year highly time-resolved measurements by an aerosol chemical speciation monitor in Beijing, China. Atmos. Chem. Phys. 18, 8469–8489.

Tiitta, P., Vakkari, V., Croteau, P., Beukes, J.P., Laakso, L., 2014. Chemical composition, main sources and temporal variability of PM_1 aerosols in southern African grassland. Atmospheric Chemistry & Physics 14, 1909–1927.

Tsai, H.-H., Yuan, C.-S., Hung, C.-H., Lin, Y.-C., 2010. Comparing physicochemical properties of ambient particulate matter of hot spots in a highly polluted air quality zone. Aerosol Air Qual. Res. 10, 331–344.

Ulbrich, I., Canagaratna, M., Zhang, Q., Worsnop, D., Jimenez, J., 2009. Interpretation of organic components from positive matrix factorization of aerosol mass spectrometric data. Atmos. Chem. Phys. 9, 2891–2918.

Wang, T., Tham, Y.J., Xue, L., Li, Q., Zha, Q., Wang, Z., Poon, S.C.N., Dubé, W.P., Blake, D.R., Louie, P.K.K., 2016. Observations of nitryl chloride and modeling its source and effect on ozone in the planetary boundary layer of southern China. Journal of Geophysical Research Atmospheres 121.

Xu, J., Zhang, Q., Chen, M., Ge, X., Ren, J., Qin, D., 2014. Chemical composition, sources, and processes of urban aerosols during summertime in Northwest China: insights from high-resolution aerosol mass spectrometry. Atmos. Chem. Phys. 14, 12593–12611.

Wu, Yangzhou, Ge, Xinlei, Wang, Junfeng, Shen, Yafei, Ye, Zhaolian, Ge, Shun, Wu, Yun, Yu, Huan, Chen, Mindong, 2018. Responses of secondary aerosols to relative humidity and photochemical activities in an industrialized environment during late winter. Atmospheric Environment 193, 66–78. https://doi.org/10.1016/j.atmosenv.2018.09.008 In this issue.

Xu, W.Q., Sun, Y.L., Chen, C., Du, W., Han, T.T., Wang, Q.Q., Fu, P.Q., Wang, Z.F., Zhao, X.J., Zhou, L.B., 2015. Aerosol composition, oxidative properties, and sources in Beijing: results from the 2014 Asia-Pacific economic cooperation summit study. Atmos. Chem. Phys. 15 (23), 23407–23455 (2015-12-10) 15.

Yan, J., Chen, L., Qi, L., Zhong, L., Chen, H., Zhao, S., 2015. Chemical characteristics of submicron aerosol particles during a long-lasting haze episode in Xiamen, China. Atmos. Environ. 113, 118–126.

Yong, J.L., Sun, Y., Qi, Z., Xue, L., Mei, L., Zhen, Z., Chan, C.K., 2017. Real-time chemical characterization of atmospheric particulate matter in China: a review. Atmos. Environ. 158, 270–304.

Zhang, Y.J., Tang, L.L., Wang, Z., Yu, H.X., Sun, Y.L., Liu, D., Qin, W., Zhang, H.L., Zhou, H.C., 2015. Insights into characteristics, sources and evolution of submicron aerosols during harvest seasons in Yangtze River Delta (YRD) region, China. Atmos. Chem. Phys. 15 (3), 9109–9154 (2015-02-06) 14.

Zhang, X., Zhang, Y., Sun, J., Yu, Y., Canonaco, F., Prévôt, A.S.H., Li, G., 2017. Chemical characterization of submicron aerosol particles during wintertime in a northwest city of China using an aerodyne aerosol mass spectrometry. Environ. Pollut. 222, 567–582.

Zhao, J., Du, W., Zhang, Y., Wang, Q., Chen, C., Xu, W., Han, T., Wang, Y., Fu, P., Wang, Z., Li, Z., Sun, Y., 2017. Insights into aerosol chemistry during the 2015 China victory Day parade: results from simultaneous measurements at ground level and 260 m in Beijing. Atmos. Chem. Phys. 17, 3215–3232. https://doi.org/10.5194/acp-17-3215-2017.

Zhou, W., Wang, Q., Zhao, X., Xu, W., Chen, C., Wei, D., Jian, Z., Canonaco, F., PréVôT, A.S.H., Fu, P., 2018. Characterization and source apportionment of organic aerosol at 260 m on a meteorological tower in Beijing, China. Atmospheric Chemistry & Physics 18, 1–34.